BIOCHEMISTRY
including biophysical chemistry & molecular biology

Article

pubs.acs.org/biochemistry

Molecular Dynamics Simulations of Iron- and Aluminum-Loaded Serum Transferrin: Protonation of Tyr188 Is Necessary To Prompt Metal Release

J. I. Mujika,*[,†] B. Escribano,[‡] E. Akhmatskaya,[‡] J. M. Ugalde,[†] and X. Lopez[†]

[†]Kimika Fakultatea, Euskal Herriko Unibertsitatea (UPV/EHU) and Donostia International Physics Center, PK 1072, 20080 Donostia, Euskadi, Spain

[‡]Basque Center for Applied Mathematics (BCAM), Alameda de Mazarredo 14, E-48009 Bilbao, Spain

Supporting Information

ABSTRACT: Serum transferrin (sTf) carries iron in blood serum and delivers it into cells by receptor-mediated endocytosis. The protein can also bind other metals, including aluminum. The crystal structures of the metal-free and metal-loaded protein indicate that the metal release process involves an opening of the protein. In this process, Lys206 and Lys296 lying in the proximity of each other form the dilysine pair or, so-called, dilysine trigger. It was suggested that the conformational change takes place due to variations of the protonation state of the dilysine trigger at the acidic endosomal pH. In 2003, Rinaldo and Field (*Biophys. J. 85*, 3485−3501) proposed that the dilysine trigger alone can not explain the opening and that the protonation of Tyr188 is required to prompt the conformational change. However, no evidence was supplied to support this hypothesis. Here, we present several 60 ns molecular dynamics simulations considering various protonation states to investigate the complexes formed by sTf with Fe(III) and Al(III). The calculations demonstrate that only in those systems where Tyr188 has been protonated does the protein undergo the conformational change and that the dilysine trigger alone does not lead to the opening. The simulations also indicate that the metal release process is a stepwise mechanism, where the hinge-bending motion is followed by the hinge-twisting step. Therefore, the study demonstrates for the first time that the protonation of Tyr188 is required for the release of metal from the metal loaded sTf and provides valuable information about the whole process.

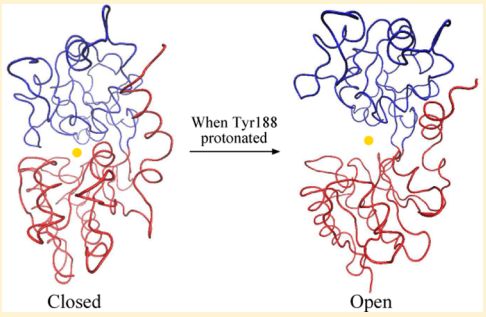

Transferrins form a family of glycoproteins whose main function is to control the level of free iron in physiological fluids by binding this element.[1] The three main proteins of this group are serum transferrin (sTf), lactoferrin (Lf), and ovotransferrin (oTf). Lf is found in such secretory fluids as milk or tears, but also in white blood cells, while oTf is present in egg white. Lf and oTf act as antimicrobial agents chelating Fe(III), which contributes to the growth of bacteria.[2−4] sTf is present in all vertebrates. It binds dietary iron, transports it in serum, and delivers it to cells through a process of receptor-mediated endocytosis.[5,6] The level of sequence similarity between members of the transferrin family is ∼60%.[1] They all possess the chain folded into two globular lobes, termed the N- and C-lobes or domains, connected by a short protein chain. The two lobes share a high degree of similarity (40%). Each lobe contains a metal binding site and is divided into two subdomains, CI and CII and NI and NII, respectively, in which a central mixed β-sheet is surrounded by several α-helices. In each lobe, two subdomains are connected by a hinge consisting of two extended antiparallel β-strands, which form a cleft where the metal can be placed.

In both the C- and N-binding sites, the metal is coordinated by an aspartic acid, two tyrosines, and a histidine. Moreover, the presence of a synergistically bound carbonate ion[7,8] is essential for metal binding. The intake of the metal by sTf is initialized by the binding of the carbonate ion to the apotransferrin present in blood serum.[9] Then the metal reaches the metal binding site of the protein, and the complex is recognized by transferrin receptor 1 (TFR) and internalized in the cytoplasm by receptor-mediated endocytosis.[10] There, release of the metal from sTf is influenced by the sTf−TFR interaction[11,12] and modulated by the lower endosomal pH of 5.5, which is significantly lower than the serum pH (7.4). In addition, several studies indicate that certain anions interact with the protein at kinetically significant anion binding (KISAB) sites, increasing the rate of metal release.[13,14]

X-ray crystal structures of the transferrin family members determine that the transferrin protein presents two different conformations, an open conformation when it is metal free[15−20] and a closed conformation upon the binding of Fe(III).[7,21−26] This conformational change involves a rigid body rotation of ∼50−64° around the hinge segment located between the two subdomains.[27,19,18] On the basis of these geometrical features, it

Received: May 4, 2012
Revised: August 4, 2012
Published: August 8, 2012

is accepted that the change in conformation upon metal release involves two global motions: hinge twist and hinge bending.[28]

The conformational change during the metal release process is not entirely understood. It was suggested that the Lys206 and Lys296 residues, located in subdomains NII and NI, respectively, modulate the opening of the metal-loaded protein by forming the so-called "dilysine trigger".[29] X-ray crystal structures show that these two residues form a hydrogen bond interaction in the iron-loaded protein,[21] while the distance between them is significantly larger in the apo form.[18] This difference was explained by a different protonation state of Lys206, neutral at physiological pH but protonated at the endosomal pH of 5.5. The repulsion between the two positively charged lysines would facilitate the opening of the domain and release of the metal. This explanation was reinforced by the fact that N-lobes of sTf and oTf release iron at higher pH values than their respective C-lobes and also than Lf, which lacks the dilysine trigger.[29,5] The importance of Lys206−Lys296 interaction was supported by several experiments in which the mutation of these residues to neutral or negatively charged residues decreases the iron release rate at pH of 5.6.[30−33] Nevertheless, some authors argued that the dilysine trigger alone cannot explain the metal release process.[9,31] Rinaldo and Field first evaluated the pK_a values of the most relevant amino acids. The pK_a value computed for Lys206 confirmed that this residue may present different protonation states in serum and in endosomes.[9] However, by performing 1.5 ns molecular dynamics simulations, the authors observed that, although the repulsion between the positively charged Lys206 and Lys296 disrupts the dilysine interaction, Lys296 still has enough room to accommodate itself without triggering the opening. In the same vein, the double mutation of Lys206 and Lys296 to Glu, causing the repulsion between negative charges of these two residues, did not lead to domain opening, as follows from the observation of the crystal structure of the mutant.[31] On the basis of all these facts, Rinaldo and Field proposed[9,31] that the electrostatic repulsion between Lys206 and Lys206 does not lead to a spontaneous domain opening and suggested that the protonation of Lys206 at the endosomal pH prompts the protonation of Tyr188 by Lys296, which would lead to a weakening of the metal binding site. However, there was no evidence supporting this hypothesis.

Only 30% of sTf is saturated by ferric iron, and the remaining sTf sites are available for other metals,[34,35] such as Al(III).[36,37] Even though this metal is not essential for the human body, human activity has increased its bioavailability, and significant traces of Al(III), whose toxic effects are still under debate, are detected today in living organisms. It was determined that 60% of the aluminum in serum is bound to sTf, 34% to albumin, and the remaining amount to citrate.[38] A computational model for aluminum in blood[39] showed a percentage of sTf-bound aluminum that was as high as ∼90%. These data indicate that sTf is the main carrier of aluminum in blood serum, and close examination of the sTf−Al(III) complexes is indispensable for understanding the effects of Al(III) on human health.

Previously, we studied the interaction of the N-lobe of sTf with Al(III) and Fe(III) under different pH conditions by performing QM/MM molecular dynamics simulations using the AM1 semiempirical method for treating the metal binding site.[40] The structures were further refined by QM/MM optimizations using high-level DFT functionals to handle the QM part. The results indicate that the mode of interaction of Al(III) and Fe(III) with sTf does change with different pH conditions. The level of theory employed in this study allowed us to investigate in detail the binding sites for both metals. However, the predictive simulation of longer events as conformational changes of a protein could not be achieved with these types of calculations. In the present work, we perform a series of 60 ns MM molecular dynamics simulations of the complexes formed by the N-lobe of sTf with Fe(III) and Al(III). Several protonation states were considered, including the protonation of Tyr188. The simulations provide valuable information for understanding the metal release process and confirm that the dilysine trigger alone does not lead to domain opening, but the protonation of Tyr188 is required to reach the conformational change.

METHODOLOGY

Gromacs (version 4.5.3)[41,42] was employed to perform all molecular dynamics simulations. In the absence of crystal structures containing the entire sequence of metal-loaded human serum transferrin, the crystal structure of the iron-loaded recombinant N-lobe (PDB entry 1AM8E)[21] was chosen as a starting configuration for all simulations. This is the reasonable choice because the N-lobe and entire molecule show similar spectroscopic, structural, iron binding, and release characteristics.[43,44] The structure contains 329 amino acids (residues 3−331) of the protein, one iron atom, and the carbonate ion. Subdomain NI comprises residues 1−93 and 247−315, whereas residues 94−246 are located in subdomain NII. The two subdomains are connected by two extended antiparallel β-strands (residues 93−103 and 243−254) that form the hinge. The metal coordination shell is composed by the synergistic carbonate ion and Asp63, Tyr188, Tyr95, and His249.

The more acidic conditions in the cell (pH 5.5) versus the physiological conditions in blood serum affect the protonation states of some residues. Most of the residues maintain the normal protonation state in both media, which is not the case for histidines. Under the physiological-pH conditions, they were considered neutral, whereas under the acidic conditions, their protonation states were updated following the criteria of Rinaldo and Field:[9] His14, His25, His242, His273, and His289 were protonated, and His119, His207, and His300 were kept neutral. As in our previous work[40] and according to the previous DFT optimizations,[45] His249 presented the imidazolate group under physiological conditions, which was neutralized under acidic conditions.

The CHARMM27 all-atom force field[46] was employed to build the topology of the protein. The nonbonded parameters of Fe(III) and Al(III) were taken from refs 47 and 48, respectively. To test the suitability of these parameters, 2 ns molecular dynamics simulations of Al(III) and Fe(III) in a box of explicit water molecules were conducted (data not shown). The octahedral coordination mode was maintained, even if starting from a nonoctahedral arrangement. Once the system was built, the steepest descents (SD) method was employed to minimize the energy of the system. Periodic boundary conditions were applied in all directions using a rhombic dodecahedron cell, with a minimal distance between the protein and the wall of the cell set to 10 Å. Then, TIP3P type water molecules[49] were added, and the system was neutralized with a NaCl concentration of 0.150 M. The energy of the entire system was again minimized with SD. A 200 ps equilibration was performed in the canonical thermodynamic ensemble (*NVT*), where the temperature of the protein and the rest of the system were independently coupled to 300 K using velocity rescaling with a stochastic term (V-rescale) algorithm.[50] The positions of the protein, carbonate, and metal atoms were weakly constrained at this stage. Long-range

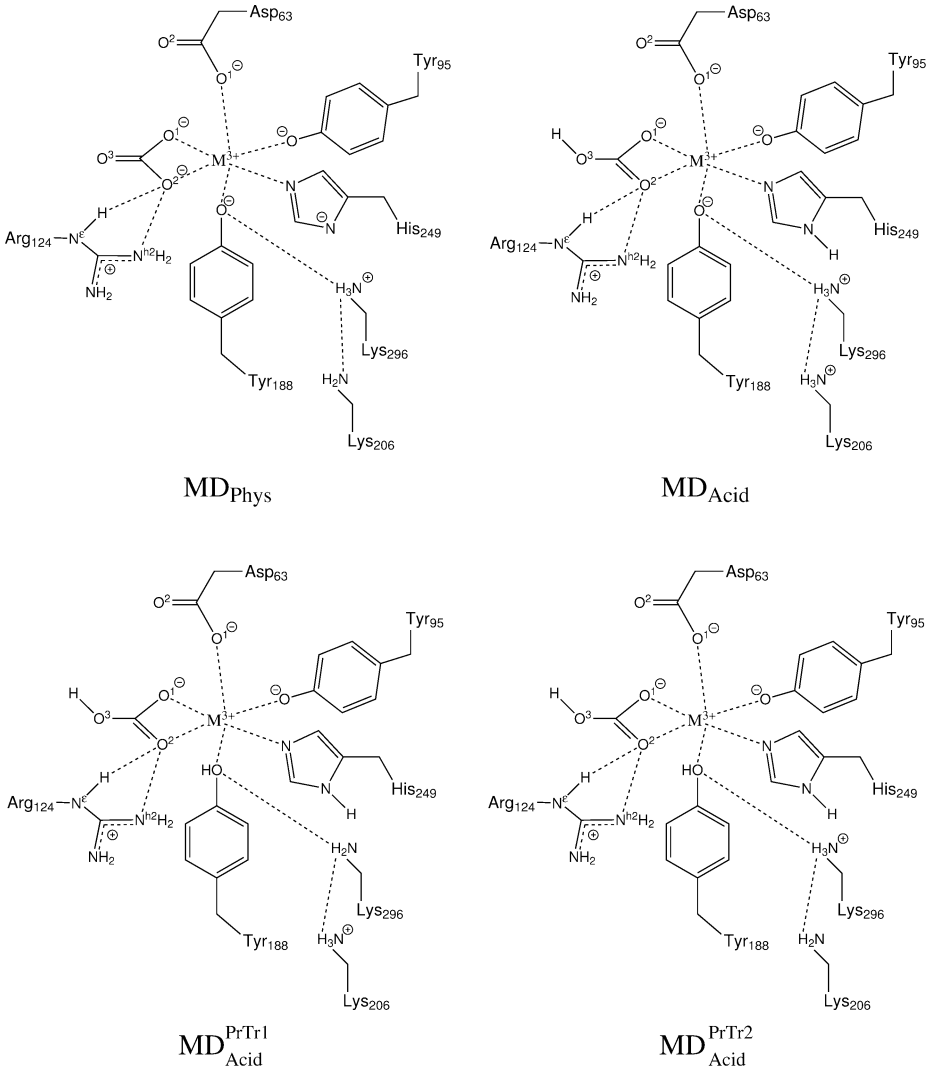

Figure 1. Schematic representation of the transferrin metal [M = Fe(III) or Al(III)] binding site for four systems considered in this work: MD_{Phys}, MD_{Acid}, MD^{PrTr1}_{Acid}, and MD^{PrTr2}_{Acid}.

electrostatics were calculated using the smooth particle mesh Ewald (PME) method[51,52] with a cutoff of 15 Å. A cutoff of 11 Å was chosen for the van der Walls nonbonded interaction where the switch function was employed. Moreover, long-range dispersion correction to the energy terms was applied to account for truncation of the van der Waals interactions. All bond lengths were constrained with Linear Constraint Solver (LINCS),[53] allowing for an integration time step of 2 fs. A total run of 60 ns was conducted for the production of each simulation under *NVT* conditions without applying any additional constraints.

RESULTS

Eight molecular dynamics simulations were performed at four different protonation states (presented in Figure 1) for the sTf–iron and sTf–aluminum complexes. In the MD_{Phys} simulations, the protonation states of the amino acids were adjusted to the pH conditions in blood serum (pH 7.4). In the rest of the simulations, MD_{Acid}, MD^{PrTr1}_{Acid}, and MD^{PrTr2}_{Acid}, the more acidic pH found in cells was considered and this difference was reflected in the protonation states of Tyr188, Lys296, and Lys206 (see below).

The root-mean-square deviations (rmsd) of the protein backbone collected from all simulations are shown in Figure 2. The radii of gyration of the protein are listed in Figure S1 of the Supporting Information, whereas the averages and standard deviations of the distances between the cations and the residues forming the first coordination shell are presented in Table S1 of the Supporting Information. In addition, other important geometrical parameters are listed in Table S2 of the Supporting Information.

Metal-Loaded sTf in Blood Serum. In the $MD_{Phys,Fe}$ and $MD_{Phys,Al}$ molecular dynamics simulations (see Figure 1), Tyr95 and Tyr188 are deprotonated, an imidazolate group is in His249, and the carbonate ion is deprotonated with a formal charge of −2. The two residues forming the dilysine trigger, Lys206 and Lys296, were considered neutral and protonated, respectively, in agreement with the pK_a values reported for these residues.[9]

$MD_{Phys,Fe}$. The rmsd is stabilized at 1 Å. The radius of gyration of the N-lobe of sTf protein is stabilized at ∼19.7 Å, which is approximately half the hydrodynamic radius of Fe_2sTf measured experimentally.[54] During the simulation, Fe(III) exhibits an octahedral coordination mode, interacting with the carbonate ion (bidentatedly), Asp63, Tyr95, Tyr188, and His249. Five of the six distances show an average value of 1.9 Å, while the Fe(III)–His249 N distance is 2.1 Å (see Table S1 of the Supporting Information).

dx.doi.org/10.1021/bi300584p | *Biochemistry* 2012, 51, 7017–7027

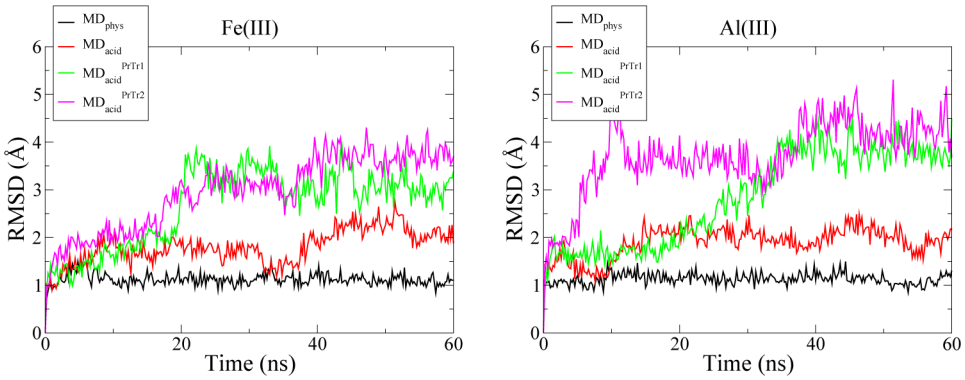

Figure 2. rmsd of the sTf backbone atoms computed during the molecular dynamics simulations considering four protonation states (MD_{Phys}, MD_{Acid}, MD^{PrTr1}_{Acid}, and MD^{PrTr2}_{Acid}) for Fe(III)−sTf (left) and Al(III)−sTf (right) complexes.

During the simulation, the interaction between the neutrally charged Lys206 and the positively charged Lys296 is stable with an average Lys206 N−Lys296 N distance of 3.0 ± 0.4 Å. Lys296 also interacts with Tyr188, and the average value for the Tyr188 O−Lys296 N distance is 2.8 ± 0.1 Å. On the other hand, Arg124 forms two hydrogen bond interactions with the O^2 atom of the carbonate ion through its N^{ε} and N^{h2} atoms. The average value of these two distances is 2.8 Å during the 60 ns production simulation. Thr120 is also forming a stable hydrogen bond interaction with CO_3 O^3, the only oxygen atom of the carbonate ion not interacting with Fe(III).

$MD_{Phys,Al}$. As for the simulation with iron, the rmsd is stabilized at 1 Å and the radius of gyration of the protein is 19.7 Å, which also corresponds to half the hydrodynamic radius measured experimentally for Al_2sTf.[54] Al(III) also adopts an octahedral coordination mode. The distances from the metal to the residues forming the metal coordination shell are on average 0.2 Å shorter than in the case of iron, indicating that the employed parameters reflect correctly the smaller radius of aluminum. The only exception is the Al(III)−His249 N distance (2.1 Å), which is very similar to the corresponding distance for iron and therefore 0.2 Å larger than the five other distances.

The second coordination sphere of Al(III) is analogous to that presented by the sTf−Fe(III) complex. The Lys206−Lys296 interaction is maintained, with a Lys206 N−Lys296 N average distance of 2.9 Å, and the Tyr188 O−Lys296 N distance is equal to 2.8 Å. As in $MD_{Phys,Fe}$, Thr120 interacts with the carbonate ion and the Thr120 O−CO_3 O^3 distance is 2.6 ± 0.0 Å.

Metal-Loaded sTf in the Cell. At the metal binding site (see Figure 1, MD_{Acid}), His249 is now neutral, the carbonate ion has gained a proton, and Lys206 bears a positive charge. Three protonation states were considered for the sTf−Fe(III) and sTf−Al(III) complexes: (i) in MD_{Acid}, Tyr188 remains unprotonated and both Lys206 and Lys296 are fully protonated; (ii) in MD^{PrTr1}_{Acid}, Tyr188 has been protonated by Lys296 and Lys206 remains positively charged; and (iii) in MD^{PrTr2}_{Acid}, Tyr188 is also protonated but now Lys206 is neutral and Lys296 positively charged.

$MD_{Acid,Fe}$. The computed rmsd is stabilized at ∼2 Å and therefore is slightly larger than in $MD_{Phys,Fe}$. The radius of gyration stabilized at 20 Å and is 0.3 Å larger than in $MD_{Phys,Fe}$. During the first 20 ns of the simulation, the iron exhibits an octahedral arrangement as in $MD_{Phys,Fe}$. The distances between Arg124 and the bicarbonate ion are larger than in $MD_{Phys,Fe}$, but in general, Arg124 presents the same interaction mode with N^{ε} and N^{h2} groups interacting mainly with the O^2 atom of the bicarbonate ion. In spite of the protonation of the carbonate ion, Thr120 maintains the hydrogen bond interaction with CO_3 O^3. His249 has gained a proton in contrast to the $MD_{Phys,Fe}$ case, and its new protonation state has weakened its interaction with Fe(III). For the first 25 ns of the simulation, the value of the Fe(III)−His249 N distance is ∼2.2 Å; however, it increases to ∼3 Å, and the average value of the distance is 2.6 ± 0.4 Å, thus 0.5 Å larger than in $MD_{Phys,Fe}$. The movement of His249 from the metal first solvation sphere under acidic conditions was also observed in the AM1/OPLS molecular dynamics simulations conducted for the Al−sTf complex.[40]

As expected, the Lys206−Lys296 distance has increased because of the repulsion between these two positively charged residues. The Lys206 N−Lys296 N distance has increased to 5.4 Å, which is 2.4 Å larger than in $MD_{Phys,Fe}$. However, as previously reported,[9,40] the disruption of the dilysine trigger does not lead to any apparent conformational change in the molecule (see below). On the other hand, Tyr188 forms a hydrogen bond interaction with Lys296 during the simulation at an average distance of 2.9 Å, and therefore, the protonation of Tyr188 by Lys296 seems plausible.

$MD_{Acid,Al}$. After simulation for a few nanoseconds, the rmsd is stabilized at ∼2 Å. Al(III) keeps its octahedral conformation during the entire simulation.

The Lys206 N−Lys296 N distance has increased to 5.6 Å, but as in $MD_{Acid,Fe}$, this disruption does not trigger any relevant conformational change in the protein. Lys296 is interacting with Tyr188 at an average distance of 2.9 Å.

$MD^{PrTr1}_{Acid,Fe}$. During a several nanosecond simulation, the rmsd value stays close to 2 Å. Then in ∼20 ns, a steep increase in the rmsd value is observed until it stabilizes at around 3.5 Å. A similar trend is also observed in the evolution of the radius of gyration, which increases from 19.7 Å at the beginning of the simulation to 20.5 Å at the end. The drastic changes observed in these two parameters indicate that an important change in conformation takes place during the simulation.

For the first 20 ns of the simulation, Fe(III) stays in an octahedral coordination mode. During this period, the Fe(III)−Tyr188 O distance is 2.2 Å, which is 0.3 Å larger than in the previous two simulations. However, after 20 ns of simulation, this distance lengthens to 5 Å. Note that this increment correlates with the change observed in the rmsd and radius of gyration values. Once Tyr188 has left the metal coordination shell, some water molecules are now in the proximity of Fe(III)

dx.doi.org/10.1021/bi300584p | *Biochemistry* 2012, 51, 7017−7027

(see Figure 5), indicating that the cation is now in a solvent accessible area (see below).

Interestingly, the protonation of Tyr188 has a strong influence on the metal second coordination sphere. After simulation for a few picoseconds, in which the N^{ε} and N^{h2} atoms of Arg124 are located ~3 Å from the bicarbonate ion, Arg124 moves away from the synergistic anion and these two distances increase by approximately 2 Å. Therefore, Arg124 leaves its original position before Tyr188 leaves the metal coordination shell (Figure 3),

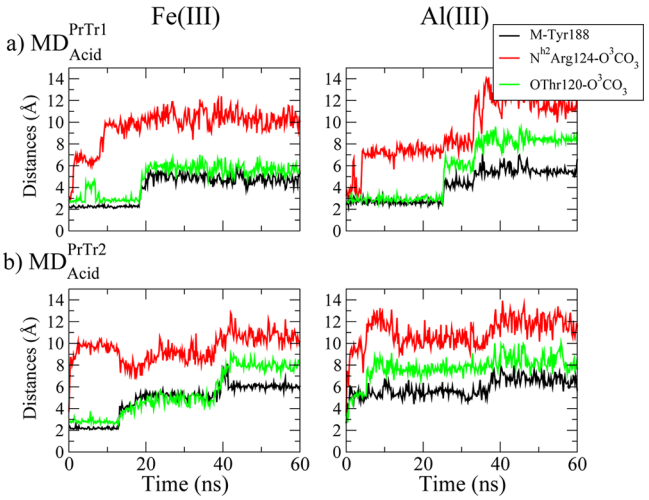

Figure 3. Evolution of three distances (in angstroms) during the MD^{PrTr1}_{Acid} (top) and MD^{PrTr2}_{Acid} (bottom) molecular dynamics simulations of Fe(III)−sTf (left) and Al(III)−sTf (right) complexes: (1) cation−Tyr188 O (black line), (2) Arg124 N^{h2}−CO_3 O^3 (red line), and (3) Thr120 O−CO_3 O^3 (green line).

which suggests that the accommodation of Tyr188 in the metal second coordination shell is possible only if Arg124 has left its original position interacting with the carbonate ion. On the other hand, in the initial stage of the simulation, Thr120 is still interacting with the bicarbonate ion, regardless of the movement of the side chain of Arg124 away from the anion. However, it begins to move away just at the moment Tyr188 leaves the first coordination shell (see Figure 3). The average value of the Thr120 O−CO_3 O^3 distance is 2 Å larger than in the previous two simulations of the Fe(III)−sTf complex.

$MD^{PrTr1}_{Acid,Al}$. The rmsd computed for the first nanosecond of the simulation is 1.5 Å; however, as in the case of iron, after simulation for 20 ns, the value starts increasing steadily, and after simulation for 35 ns, it is stabilized at around 4 Å. The radius of gyration shows a similar trend and goes from 19.7 Å at the beginning of the simulation to 20.8 Å after 35 ns of simulation.

For the first 25 ns of the simulation, Al(III) keeps an octahedral arrangement interacting with Asp63, Tyr95, Tyr188, and the bicarbonate ion. However, at the time in which the values of rmsd and radius of gyration increase, the Al(III)−Tyr188 O distance lengthens to 4 Å first, to be stabilized at ~5 Å at the end of the simulation. Therefore, as in $MD^{PrTr1}_{Acid,Fe}$, the change in conformation is correlated with the departure of Tyr188 from the cation coordination shell. Interestingly, once Tyr188 leaves the metal coordination shell, Al(III) maintains a hexacoordinated arrangement because of the inclusion of a water molecule in its solvation sphere (see Figure 5). In the new rearrangement, the water molecule and Tyr95 are placed in axial positions and the bidentate bicarbonate ion, Asp63, and His249 occupy the equatorial positions.

As it was observed in the $MD^{PrTr1}_{Acid,Fe}$ simulation, the departure of Tyr188 is preceded by the departure of Arg124 from the vicinity of the bicarbonate ion (see Figure 3). The Arg124 N^{h2}−CO_3 O^3 distance lengthens to 7 Å first and to 10 Å when Tyr188 leaves the metal coordination shell. The interaction of Thr120 with the bicarbonate ion is also broken when Tyr188 moves away from the metal coordination shell.

$MD^{PrTr2}_{Acid,Fe}$. The evolutions of the rmsd and radius of gyration observed during the $MD^{PrTr2}_{Acid,Fe}$ simulation are similar to those observed during the $MD^{PrTr1}_{Acid,Fe}$ simulation. Thus, an important increment in their values appears after simulation for a few nanoseconds, indicating that a conformational change has occurred. During the first few nanoseconds, Tyr188 remains bound to the iron, but after simulation for approximately 12 ns, the residue leaves the metal first coordination shell to be placed in the second shell, behind the bicarbonate ion. The average value of the Fe−Tyr188 O distance is 4.8 ± 1.5 Å, which is 3 Å larger than in $MD_{Acid,Fe}$. Once Tyr188 leaves the iron coordination sphere, Asp63 changes its interaction mode from monodentate to bidentate and the Fe−Asp63 O^2 average distance is reduced to 2.5 Å, thus becoming 1.5 Å shorter than in $MD_{Acid,Fe}$. Moreover, a water molecule has been introduced into the metal coordination sphere. Therefore, the bicarbonate ion, Asp63 (both bidentate) and His249 are placed in the equatorial plane, whereas the water molecule and Tyr95 are in axial positions.

As in $MD^{PrTr1}_{Acid,Fe}$, the protonation of Tyr188 produced an immediate displacement of Arg124 from the vicinity of the bicarbonate. Nevertheless, Thr120 interacts with the synergistic anion until Tyr188 moves away (see Figure 3). Moreover, because of the protonation of Lys296, this residue does not interact with Tyr188 and the distance between them lengthens to 7.0 Å. On the other hand, an important movement of Lys206 is observed, not seen in the $MD^{PrTr1}_{Acid,Fe}$ simulation. Lys206 approaches the bicarbonate ion to interact with its OH group because of its neutral charge and perhaps because of the room provided by a movement of Arg124 toward the bicarbonate ion. The Lys206 N−CO_3 O^3 distance reduces to an average value of 4.2 Å; this is 5 Å shorter than in $MD_{Acid,Fe}$.

$MD^{PrTr2}_{Acid,Al}$. The computed rmsd and radius of gyration also give evidence of a conformational change during the simulation. Tyr188 has left the aluminum coordination shell at the very beginning of the simulation. Although the final global conformation of the protein is analogous to that observed in $MD^{PrTr2}_{Acid,Fe}$, it is worth noting that the final coordination mode of aluminum is different from that of iron, because Asp63 maintains its monodentate interaction mode (the Asp63 O^2 average distance is 3.5 Å, which is 1.0 Å larger than in the simulation with iron). Note that this difference in the coordination of Asp63 in the presence of different metals, iron or aluminum, was also observed in the QM/MM molecular dynamics simulation and in posterior QM/MM optimizations.[40] The position of Tyr188 in the metal coordination mode has been replaced with a water molecule, and therefore, Al(III) still adopts an octahedral coordination mode in which His249, Tyr95, and the bicarbonate ion are in the equatorial plane and Asp63 and a water molecule are in axial positions.

As in the case of the simulation with iron, Arg124 leaves its position because of the interaction with the bicarbonate ion, which is confirmed by increasing average values of the N^{ε}−O^3 and N^{h2}−O^2 distances. The interaction between Thr120 and the bicarbonate ion is also disrupted. Even if only one of the lysines is positively charged, the Lys206−Lys296 interaction is

dx.doi.org/10.1021/bi300584p | *Biochemistry* 2012, 51, 7017−7027

not recovered (their average distance is more than 7 Å). Instead, Lys206 has approached the bicarbonate ion with the Lys206 N−CO_3 O^3 distance shortened to 4.2 ± 1.1 Å.

Principal Component Analysis. The dynamics of the protein during the molecular dynamics simulations includes local and collective motions, which are difficult to distinguish by visual examination of the trajectories. To identify these global motions, principal component analysis (PCA), also known as essential dynamics simulation, can be efficiently applied. In PCA, the 3N coordinates of the protein are transformed into a new set of eigenvectors, called principal components, and the eigenvalues of these vectors provide the amplitudes of the motion. Usually, a few of these principal components are sufficient to account for the majority of the global motions accumulated in the trajectory of the molecular dynamics simulation. In Table 1, the eigenvalues of the first five principal components corresponding to the backbone protein for all performed simulations are presented.

Table 1. Eigenvalues of the First Five Principal Components Calculated for Eight MD Production Simulations Run over 60 ns[a]

eigenvalue	MD_{Phys}	MD_{Acid}	MD_{Acid}^{PrTr1}	MD_{Acid}^{PrTr2}
		Iron		
1	0.64 (14.5)	2.45 (22.9)	10.05 (60.4)	15.86 (65.7)
2	0.33 (7.4)	2.23 (20.8)	1.29 (7.8)	2.64 (10.9)
3	0.22 (4.9)	1.15 (10.7)	0.98 (5.9)	0.72 (3.0)
4	0.19 (4.3)	0.57 (5.4)	0.44 (2.7)	0.41 (1.7)
5	0.14 (3.2)	0.41 (3.8)	0.41 (2.4)	0.33 (1.4)
		Aluminum		
1	0.48 (11.4)	1.47 (20.0)	21.11 (75.9)	7.56 (53.9)
2	0.39 (9.4)	1.27 (17.2)	1.81 (6.5)	1.31 (9.4)
3	0.23 (5.4)	0.59 (8.0)	0.59 (2.1)	0.87 (6.2)
4	0.18 (4.3)	0.36 (4.8)	0.48 (1.7)	0.42 (3.0)
5	0.17 (4.2)	0.30 (4.1)	0.33 (1.2)	0.26 (1.8)

[a]The amount of mobility (in percent) captured by each principal component in the corresponding simulation is shown in parentheses.

The first conclusion from the data collected in Table 1 is that the modes computed in the MD_{Acid}^{PrTr1} and MD_{Acid}^{PrTr2} simulations are significantly larger than in MD_{Phys} and MD_{Acid}, for both metals, iron and aluminum. This means that in the simulations with the protonated Tyr188, the protein is more mobile. Moreover, the amount of mobility captured by the first principal component (shown in parentheses in Table 1) is significantly larger in the MD_{Acid}^{PrTr1} and MD_{Acid}^{PrTr2} simulations than in the other two systems. In the simulations with iron, the first principal component captures 14.5% of the motion accumulated in $MD_{Phys,Fe}$ and 22.9% in $MD_{Acid,Fe}$, while in $MD_{Acid,Fe}^{PrTr1}$ and $MD_{Acid,Fe}^{PrTr2}$, the contribution increases to 60.4 and 65.7%, respectively. In the case of aluminum, the first mode is also predominant, and the first principal components account for 75.9 and 53.9% of the fluctuations stored in $MD_{Acid,Al}^{PrTr1}$ and $MD_{Acid,Al}^{PrTr2}$, respectively. In contrast, the values are small in $MD_{Phys,Al}$ and $MD_{Acid,Al}$.

The coordinates of the trajectories were projected out along the selected principal components. The visual analysis of these projections indicates that in those four simulations in which Tyr188 is protonated, i.e., MD_{Acid}^{PrTr1} and MD_{Acid}^{PrTr2} systems with iron and aluminum, the first principal component represents the hinge-bending motion. On the other hand, the second principal component accounts for ∼10% of the motion accumulated in these four simulations and the motion involves the hinge-twisting step.

Opening of the Protein. PCA reveals that hinge bending is the main global motion in the MD_{Acid}^{PrTr1} and MD_{Acid}^{PrTr2} simulations, but not in MD_{Phys} and MD_{Acid}. To further investigate and quantify this motion, the distance between the centers of mass of the NI and NII subdomains has been monitored for all eight MD simulations (shown in Figure 4) and compared with those of X-ray crystal structures.

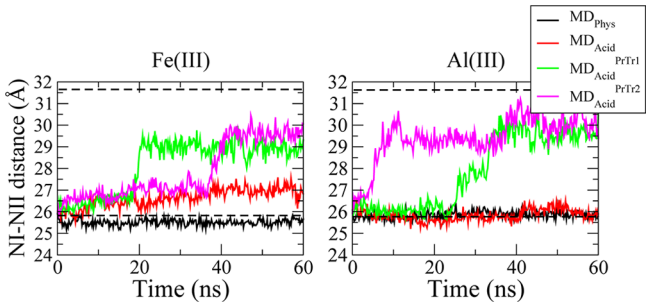

Figure 4. Distance between the centers of mass of subdomains NI and NII measured during the molecular dynamics simulations with four protonation states (MD_{Phys}, MD_{Acid}, MD_{Acid}^{PrTr1}, and MD_{Acid}^{PrTr2}) considered for Fe(III)−sTf (left) and Al(III)−sTf (right) complexes. The dashed lines refer to the values in the crystal structures of the iron-loaded form and apo form of sTf.

The NI−NII distance measured in the crystal structure is 25.9 Å for sTf loaded with iron[21] and 31.6 Å in the crystal structure of the apo form.[18] During the MD_{Phys} and MD_{Acid} simulations with aluminum, the average value of this distance is almost identical to the value in the iron-loaded crystal structure. In the simulations with iron, the distance is slightly larger in MD_{Acid} and shorter in MD_{Phys}, though with only a small deviation. On the other hand, during the remaining four simulations (MD_{Acid}^{PrTr1} and MD_{Acid}^{PrTr2} systems), the distance increases to 29−30 Å. Note that there is a correlation among the behavior of this distance, the rmsd, and radius of gyration, indicating that the opening of the protein is the main initiator of the conformational change.

To confirm that the change in conformation of the protein facilitates the inclusion of the solvent in the cleft, two parameters have been measured (shown in Figure S1 of the Supporting Information): the solvent accessible surface (SAS) of the protein and the radial distribution function [$g(r)$] of water molecules around the metal. The comparison among all eight simulations shows that the SAS of the protein increases when the protein changes to a more open conformation, especially in the $MD_{Acid,Fe}^{PrTr2}$ simulation. In the four simulations with Tyr188 deprotonated, the values of $g(r)$ are close to zero for distances of <10 Å. On the other hand, in the simulations with protonated Tyr188, the values of $g(r)$ are significantly higher in the proximity of the cation. In fact, at a distance of 2 Å, $g(r)$ is equal to 2 and 1 for the cases of Fe(III) and Al(III), respectively. This is in agreement with the number of water molecules found in the metal coordination shell in the final structure of these simulations (see Figure 5). In summary, all these data indicate that the opening of the protein has provided an access of the solvent to the metal, allowing the cation to leave the metal binding site.

DISCUSSION

In the $MD_{Acid,Fe}$ and $MD_{Acid,Al}$ simulations, where Lys206 and Lys296 bear a positive charge and the electrostatic repulsion between them has disrupted the interaction, the protein retains the closed conformation. The same behavior, observed by

dx.doi.org/10.1021/bi300584p | Biochemistry 2012, 51, 7017−7027

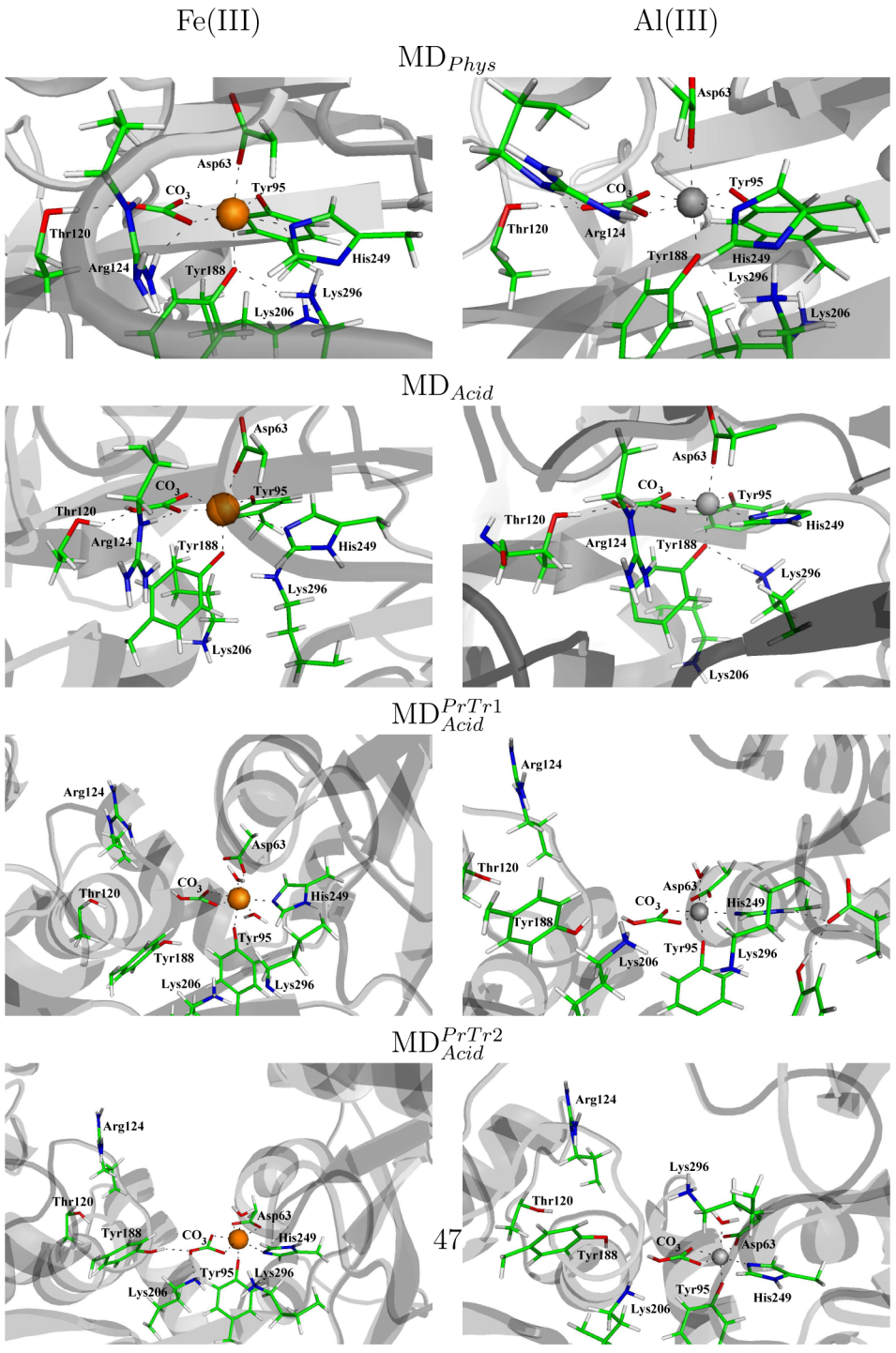

Figure 5. Representative snapshots of the molecular dynamics simulations with four protonation states (MD_{Phys}, MD_{Acid}, MD^{PrTr1}_{Acid}, and MD^{PrTr2}_{Acid}) considered for Fe(III)−sTf (left) and Al(III)−sTf (right) complexes.

Rinaldo and Field,[9] led them to the conclusion that the side chains of two lysines have enough room to accommodate themselves without triggering the conformational change. These results therefore confirm that the breaking of the dilysine trigger is insufficient to prompt the opening of the protein and an additional step is necessary to induce opening.

In that vein, it was proposed that the protonation of Lys206 at lower pH values may facilitate the protonation of Tyr188 by Lys296,[9,31] which in turn would weaken the interaction between the protein and the metal. A pK_a of 4.1 was theoretically calculated by our group for the Al(III)-bound tyrosine,[55] whereas a value of 6.85 ± 0.05 was determined on the basis of the ^{13}C chemical shift in apo-hTF/2N.[56] These values indicate that the protonation of Tyr188 is more likely to happen at the endosomal pH of 5.5 than at physiological pH. In four MD simulations with the protonated Tyr188 (MD^{PrTr1}_{Acid} and MD^{PrTr2}_{Acid} systems in Figure 1), the relevant rearrangement of the protein is observed and confirmed by the drastic increase in both the rmsd and the radius of gyration. The analysis of the simulations confirms that these rearrangements correspond to the opening of the protein

dx.doi.org/10.1021/bi300584p | *Biochemistry* 2012, 51, 7017−7027

(see below). Because this conformational change was not observed in those four molecular dynamics simulations where Tyr188 was deprotonated, the simulations demonstrate that the protonation of Tyr188 facilitates the opening of the protein prior to metal release.

The molecular dynamics simulations also provide relevant information about the critical amino acids, such as Tyr188, Arg124, Lys206, and Lys296. In those simulations where Tyr188 is deprotonated, this amino acid is tightly bound to the metal. On the other hand, Arg124 and Thr120 are placed in the metal second coordination sphere, forming stable hydrogen bonds with the carbonate ion. However, when Tyr188 is neutralized, the first immediate effect is not its departure from the metal coordination shell but the departure of Arg124 from its position interacting with the synergistic carbonate anion. Nevertheless, this displacement does not lead to any relevant conformational change in the protein, because the side chain of Arg124 has enough room for accommodation in the cleft between two subdomains. Once Arg124 has left its position near the bicarbonate ion, Tyr188 has enough space to relocate to the second shell. It is only then that the protein starts opening, as it is corroborated by the increments in the rmsd, radius of gyration, and NI−NII distance. These results therefore indicate that the protonation of Tyr188 not only weakens its interaction with the metal but also has a direct influence on the second coordination shell, which ultimately triggers the conformational change of the protein. This finding may suggest that metal release is impossible without protonation of Tyr188 first.

The performed PCAs do not identify any predominant global motions in the simulations with deprotonated Tyr188, but instead, they confirm that the hinge-bending motion is the main global motion when Tyr188 has been protonated. This finding is further supported by the larger distance between the centers of mass of subdomains NI and NII (Figure 4) in those systems where Tyr188 has been protonated. In fact, this distance is closer to its value in the apo form crystal structure than in the iron-loaded structure. The hinge-bending predominant motion in the metal-loaded sTf reported in this work differs from the hinge-twisting motion that is the most important global motion of the apo form of sTf.[9] This difference may suggest that the metal release (or binding) process is a stepwise mechanism. If one starts from the closed conformation of the metal-loaded protein, the first step would be the hinge-bending motion. This motion allows the access of the solvent to the metal binding site, as indicated by the larger solvent accessible area computed in the MD_{Acid}^{PrTr1} and MD_{Acid}^{PrTr2} (Figure S2 of the Supporting Information). Once the metal is in a solvent accessible area, the release of the metal would be facilitated by the hinge-twisting motion of the protein. Note that the final protonation states of Tyr188, Lys296, and probably Lys206 correspond to those found in the apo form under physiological conditions. This two-step mechanism was previously suggested by Grossmann et al.[28] They characterized the structures of the apo form, the holo form of wild-type sTf, and also several mutants. In two of these mutated structures, Y95H and D63S, the intermediate state was identified, which presents a hinge twist of 20° from the open conformation of the apo form, but no hinge-bending motion was observed. This intermediate structure is in agreement with our molecular dynamics simulations of the holo form of sTf, in which only the hinge bend is observed. The existence of the intermediate in the metal intake or release process was also reported previously.[57] More recently, a fluorescence study of the release of iron from the N-lobe of sTf confirms that it is a two-step process,[58] although the authors proposed the opposite order, that is, metal release followed by the conformational change in the protein.

In general, the simulations conducted with Fe(III) and Al(III) show the same global motion of the protein, which may indicate that the molecular mechanism of the release of metal from protein is analogous for both cations. They also demonstrated that Tyr188 must be protonated prior to cation release. Nevertheless, a number of differences have been identified at the atomic level between the simulations of the Fe(III)−sTf and Al(III)−sTf complexes. Some of these differences are due to the fact that the simulations explore different subspaces, and that not all of them lead to the same final conformations. However, it must take into account the fact that the entire system, including the cation, has been modeled with a nonpolarizable force field. This treatment does not allow any transfer of charge between the cation and its ligands, and therefore, the mode of coordination of the metal must be considered with caution. Nevertheless, the main aim of the study is to investigate the motion of the protein under different conditions (i.e., different protonation states), which is achieved by long molecular dynamics simulations employing a reliable force field. In the $MD_{Acid,Fe}^{PrTr2}$ simulations conducted with Fe(III) and Al(III), different coordination modes of the cation were observed. Once Tyr188 leaves the metal coordination shell, Asp63 changes its interaction mode from mono- to bidentate in the simulations with Fe(III), while the monodentate interaction mode is maintained with Al(III). This difference was previously observed in the DFT/MM calculations conducted for these two complexes[40] and may reflect an important difference between the release processes of the two metals. In the same work,[40] AM1/MM molecular dynamics simulations of the Al(III)−sTf complex were also conducted. Under acidic conditions, in which His249 was neutral, this residue left the metal coordination shell, which was observed in $MD_{Acid,Fe}$. This movement might indicate that the metal release is a complex process in which the lower endosomal pH values lead simultaneously to the weakening of the His249−metal interaction and to the protonation of Tyr188. This work shows that the latter is the key step in the opening of the protein.

The importance of Arg124 in the metal release process was previously inferred from crystal structure studies of several mutants,[59] in which Arg124 was trapped in two different positions: (i) directly interacting with the carbonate ion and (ii) more distant from the anion. Representative pictures from eight molecular dynamics simulations performed in this work are superimposed in Figure 6. There, it can be observed that in the simulations with the deprotonated Tyr188 (blue and green

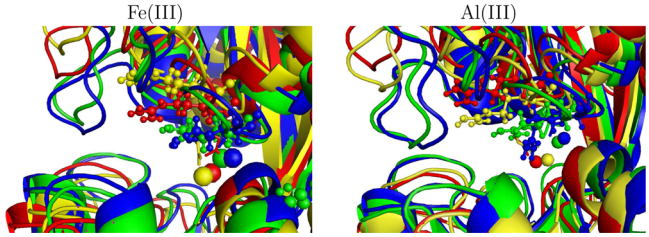

Figure 6. Superposition of representative snapshots of the molecular dynamics simulations with four protonation states considered for Fe(III)−sTf (left) and Al(III)−sTf (right) complexes: MD_{Phys} (blue), MD_{Acid} (green), MD_{Acid}^{PrTr1} (red), and MD_{Acid}^{PrTr2} (yellow). Arg124 is shown as balls and sticks, and the metal is shown as balls. Figures were prepared with Pymol.[60]

structures), Arg124 is placed at the bottom of the cleft and interacts with the synergistic carbonate anion. However, when Tyr188 has been protonated (red and yellow structures), Arg124 has moved away from the cation and toward the cleft entrance. As a consequence, a loop of the protein structure (the segment of residues 180−190) has been displaced and the metal binding site is more exposed to the solvent. These results therefore confirm the active role of Arg124 in metal release by allowing various configurations throughout the process.

CONCLUSIONS

The release of metal from an Fe(III)- and Al(III)-loaded N-lobe of serum transferrin has been investigated by molecular dynamics simulations. The calculations confirm that the protonation of Tyr188 is indispensable for prompting the conformational change of the protein. They also provide details about the metal release process. In this sense, the neutralization of Tyr188 not only weakens its interaction with the cation but also has a direct influence on Arg124. When Tyr188 has been protonated, Arg124 leaves its position interacting with the carbonate. This event has been shown to be crucial in triggering the opening of the protein.

The simulations confirm that metal release is a multistep process, initialized by the hinge-bending motion of the protein to form an intermediate state. At this stage, the protein has been partially opened but the metal is still bound to the protein. The next step implies the hinge-twisting, in which the metal would definitively leave the protein binding site.

ASSOCIATED CONTENT

Supporting Information

Tables showing mean and standard deviation values for distances between the metal and its first shell ligands and between first and second shell amino acids and figures showing radii of gyration of sTf, solvent accessible areas (SAS) of sTf, and radial distribution functions $[g(r)]$ of water molecules around the metal. This material is available free of charge via the Internet at http://pubs.acs.org.

AUTHOR INFORMATION

Corresponding Author

*Kimika Fakultatea, Euskal Herriko Unibertsitatea (UPV/EHU) and Donostia International Physics Center, PK 1072, 20080 Donostia, Euskadi, Spain. Telephone: +34 943015341. E-mail: joni.mujika@ehu.es.

Funding

This research was funded by Eusko Jaurlaritza (the Basque Government, GIC 07/85 IT-330-07) and the Spanish Ministerio de Ciencia e Innovacion (CTQ2011-27374). The SGI/IZO-SGIker UPV/EHU is acknowledged for computational resources. We are also grateful to the British Engineering and Physical Sciences Research Council (EPSRC EP/J004146/1) for financial support.

Notes

The authors declare no competing financial interest.

ABBREVIATIONS

sTf, serum transferrin; Lf, lactoferrin; oTf, ovotransferrin; MM, molecular dynamics; QM/MM, quantum mechanics/molecular mechanics; PDB, Protein Data Bank; rmsd, root-mean-square deviation; MD, molecular dynamics.

REFERENCES

(1) Sun, H. Z., Li, H. Y., and Sadler, P. J. (1999) Transferrin as a metal ion mediator. *Chem. Rev. 99*, 2817−2842.

(2) Brock, J. H. (2002) The physiology of lactoferrin. *Biochem. Cell Biol. 80*, 1−6.

(3) Weinberg, E. D. (1974) Iron and susceptibility to infectious disease. *Science 184*, 952−956.

(4) Lönnerdal, B., and Iyer, S. (1995) Lactoferrin: Molecular structure and biological function. *Annu. Rev. Nutr. 15*, 93−110.

(5) Klausner, R. D., Ashwell, G., Vanrenswoude, J., Harford, J. B., and Bridges, K. R. (1983) Binding of apotransferrin to K562 cells: Explanation of the transferrin cycle. *Proc. Natl. Acad. Sci. U.S.A. 80*, 2263−2266.

(6) Aisen, P. (1998) in *Metal ions in biological systems* (Sigel, A., and Sigel, H., Eds.) Vol. 35, pp 585−631, CRC Press, Boca Raton, FL.

(7) Anderson, B. F., Baker, H. M., Norris, G. E., Rice, D. W., and Baker, E. N. (1989) Structure of human lactoferrin: Crystallographic structure-analysis and refinement at 2.8 Å resolution. *J. Mol. Biol. 209*, 711−734.

(8) Baker, E. N. (1994) Structure and reactivity of transferrins. *Adv. Inorg. Chem. 41*, 389−463.

(9) Rinaldo, D., and Field, M. J. (2003) A computational study of the open and closed forms of the N-lobe human serum transferrin apoprotein. *Biophys. J. 85*, 3485−3501.

(10) Dautry-Varsat, A., Ciechanover, A., and Lodish, H. F. (1983) pH and the recycling of transferrin during receptor mediated endocytosis. *Proc. Natl. Acad. Sci. U.S.A. 80*, 2258−2262.

(11) Eckenroth, B. E., Steere, A. N., Chasteen, N. D., Everse, S. J., and Mason, A. B. (2011) How the binding of human transferrin primes the transferrin receptor potentiating iron release at endosomal pH. *Proc. Natl. Acad. Sci. U.S.A. 108*, 13089−13094.

(12) Steere, A. N., Chasteen, N. D., Miller, B. F., Smith, V. C., Macgillivray, R. T. A., and Mason, A. B. (2012) Structure-based mutagenesis reveals critical residues in the transferrin receptor participating in the mechanism of pH-induced release of iron from human serum transferrin. *Biochemistry 51*, 2113−2121.

(13) Amin, E. A., Harris, W. R., and Welsh, W. J. (2004) Identification of possible kinetically significant anion-binding sites in human serum transferrin using molecular modeling strategies. *Biopolymers 73*, 205−215.

(14) Byrne, S. L., Steere, A. N., Chasteen, N. D., and Mason, A. B. (2010) Identification of a kinetically significant anion binding (KISAB) site in the N-lobe of human serum transferrin. *Biochemistry 49*, 4200−4207.

(15) Kurokawa, H., Dewan, J. C., Mikami, B., Sacchettini, J. C., and Hirose, M. (1999) Crystal structure of hen apo-ovotransferrin. Both lobes adopt an open conformation upon loss of iron. *J. Biol. Chem. 274*, 28445−28452.

(16) Rawas, A., Muirhead, H., and Williams, J. (1997) Structure of apo duck ovotransferrin: The structures of the N and C lobes are in the open form. *Acta Crystallogr. D53*, 464−468.

(17) Kumar, P., Khan, J. A., Yadav, S., and Singh, T. P. (2002) crystal structure of equine apolactoferrin at 303 K providing further evidence of closed conformations of N and C lobes. *Acta Crystallogr. D58*, 225−232.

(18) Jeffrey, P. D., Bewley, M. C., MacGillivray, R. T., Mason, A. B., Woodworth, R. C., and Baker, E. N. (1998) Ligand-induced conformational change in transferrins: Crystal structure of the open form of the N-terminal half-molecule of human transferrin. *Biochemistry 37*, 13978−13986.

(19) Wally, J., Halbrooks, P. J., Vonrhein, C., Rould, M. A., Everse, S. J., Mason, A. B., and Buchanan, S. (2006) The crystal structure of iron-free human serum transferrin provides insight into inter-lobe communication and receptor binding. *J. Biol. Chem. 281*, 24934−24944.

(20) Jameson, G. B., Anderson, B. F., Norris, G. E., Thomas, D. H., and Baker, E. N. (1999) Structure of human apolactoferrin at 2.0 Å resolution. Refinement and analysis of ligand-induced conformational change. Addendum. *Acta Crystallogr. D55*, 1108.

(21) MacGillivray, R. T., Moore, S. A., Chen, J., Anderson, B. F., Baker, H., Luo, Y., Bewley, M., Smith, C. A., Murphy, M. E., Wang, Y., Mason, A. B., Woodworth, R. C., Brayer, G. D., and Baker, E. N. (1998) Two high-resolution crystal structures of the recombinant N-lobe of human transferrin reveal a structural change implicated in iron release. *Biochemistry 37*, 7919−7928.
(22) Kurokawa, H., Mikami, B., and Hirose, M. (1995) Crystal structure of diferric hen ovotransferrin at 2.4 Å resolution. *J. Mol. Biol. 254*, 196−207.
(23) Rawas, A., Muirhead, H., and Williams, J. (1996) Structure of diferric duck ovotransferrin at 2.35 Å resolution. *Acta Crystallogr. D52*, 631−640.
(24) Moore, S. A., Anderson, B. F., Groom, C. R., Haridas, M., and Baker, E. N. (1997) Three-dimensional structure of diferric bovine lactoferrin at 2.8 Å resolution. *J. Mol. Biol. 274*, 222−236.
(25) Hall, D. R., Leonard, G. A., Neu, M., and Lindley, P. F. (2002) The crystal and molecular structures of diferric porcine and rabbit serum transferrins at resolutions of 2.15 and 2.60 Å, respectively. *Acta Crystallogr. D58*, 70−80.
(26) Thakurta, P. G., Dasgupta, R., and Dattagupta, J. K. (2003) Structure of diferric hen serum transferrin at 2.8 Å resolution. *Acta Crystallogr. D59*, 1773−1781.
(27) Gerstein, M., Anderson, B. F., Norris, G. E., Baker, E. N., Lesk, A. M., and Chothia, C. (1993) Domain closure in lactoferrin: Two hinges produce a see-saw motion between alternative close-packed interfaces. *J. Mol. Biol. 234*, 357−372.
(28) Grossmann, J. G., Crawley, J. B., Strange, R. W., Patel, K. J., Murphy, L. M., Neu, M., Evans, R. W., and Hasnain, S. S. (1998) The nature of ligand-induced conformational change in transferrin in solution. An investigation using X-ray scattering, XAFS and site-directed mutants. *J. Mol. Biol. 279*, 461−472.
(29) Dewan, J. C., Mikami, B., Hirose, M., and Sacchettini, J. C. (1993) Structural evidence for a pH-sensitive dilysine trigger in the hen ovotransferrin N-lobe: Implications for transferrin iron release. *Biochemistry 32*, 11963−11968.
(30) He, Q. Y., Mason, A. B., Tam, B. M., MacGillivray, R. T. A., and Woodworth, R. C. (1999) Dual role of Lys206-Lys296 interaction in human transferrin N-lobe: Iron-release trigger and anion-binding site. *Biochemistry 38*, 9704−9711.
(31) Baker, H. M., Nurizzo, D., Mason, A. B., and Baker, E. N. (2007) Structures of two mutants that probe the role in iron release of the dilysine pair in the N-lobe of human transferrin. *Acta Crystallogr. D63*, 408−414.
(32) Steinlein, L. M., Ligman, C. M., Kessler, S., and Ikeda, R. A. (1998) Iron release is reduced by mutations of lysines 206 and 296 in recombinant N-termini half-transferrin. *Biochemistry 37*, 13696−13703.
(33) Nurizzo, D., Baker, H. M., He, Q. Y., MacGillivray, R. T. A., Mason, A. B., Woodworth, R. C., and Baker, E. N. (2001) Crystal structures and iron release properties of mutants (K206A and K296A) that abolish the dilysine interaction in the N-lobe of human transferrin. *Biochemistry 40*, 1616−1623.
(34) Harris, W. R. (1996) Binding and transport of aluminum by serun proteins. *Coord. Chem. Rev. 149*, 347−365.
(35) Ichimura, K., Kihara, H., Yamamura, T., and Satake, K. (1989) Negative cooperativity of chicken ovotransferrin on Al(III)-binding. *J. Biochem. 106*, 50−54.
(36) Martin, R. B., Savory, J., Brown, S., Bertholf, R. L., and Wills, M. R. (1987) Transferrin binding of Al^{3+} and Fe^{3+}. *Clin. Chem. 33*, 405−407.
(37) Cochran, M., Coates, J., and Neoh, S. (1984) The competitive-equilibrium between aluminum and ferric ions for the binding-sites of transferrin. *FEBS Lett. 176*, 129−132.
(38) Fatemi, S. J. A., Kadir, F. H. A., and Moore, G. R. (1991) Aluminium transport in blood serum. *Biochem. J. 280*, 527−532.
(39) Beardmore, J., Rugg, G., and Exley, C. (2007) A systems biology approach to the blood-aluminium problem: The application and testing of a computational model. *J. Inorg. Biochem. 101*, 1187−1191.
(40) Mujika, J. I., Lopez, X., Rezabal, E., Castillo, R., Marti, S., Moliner, V., and Ugalde, J. M. (2011) A QM/MM study of the complexes formed by aluminum and iron with serum transferrin at neutral and acidic pH. *J. Inorg. Biochem. 105*, 1446−1456.
(41) Hess, B., Kutzner, C., Van der Spoel, D., and Lindahl, E. (2008) Gromacs 4: Algorithms for highly efficient, load-balanced, and scalable molecular simulation. *J. Chem. Theory Comput. 4*, 435−447.
(42) Van Der Spoel, D., Lindahl, E., Hess, B., Groenhof, G., Mark, A. E., and Berendsen, H. J. C. (2005) Gromacs: Fast, flexible, and free. *J. Comput. Chem. 26*, 1701−1718.
(43) Funk, W. D., MacGillivray, R. T. A., Mason, A. B., Brown, S. A., and Woodworth, R. C. (1990) Expression of the amino-terminal half-molecule of human serum transferrin in cultured cells and characterization of the recombinant protein. *Biochemistry 29*, 1654−1660.
(44) Li, Y., Harris, W. R., Maxwell, A., MacGillivray, R. T., and Brown, T. (1998) Kinetic studies on the removal of iron and aluminum from recombinant and site-directed mutant N-lobe half transferrins. *Biochemistry 37*, 14157−14166.
(45) Rinaldo, D., and Field, M. J. (2004) A density functional theory study of the iron-binding site of human serum transferrin. *Aust. J. Chem. 57*, 1219−1222.
(46) MacKerell, A. D., Jr., Bashford, D., Bellott, M., Dunbrack, R. L., Jr., Evanseck, J. D., Field, M. J., Fischer, S., Gao, J., Guo, H., Ha, S., Joseph-McCarthy, D., Kuchnir, L., Kuczera, K., Lau, F. T. K., Mattos, C., Michnick, S., Ngo, T., Nguyen, D. T., Prodhom, B., Reiher, W. E., Roux, B., Schlenkrich, M., Smith, J. C., Stote, R., Straub, J., Watanabe, M., Wiórkiewicz-Kuczera, J., Yin, D., and Karplus, M. (1998) All-atom empirical potential for molecular modeling and dynamics studies of proteins. *J. Phys. Chem. B 102*, 3586−3616.
(47) Faro, T. M. C., Thim, G. P., and Skaf, M. S. (2010) A Lennard-Jones plus Coulomb potential for Al^{3+} ions in aqueous solutions. *J. Chem. Phys. 132*, 114509−114516.
(48) Lin, W., Welsh, W. J., and Harris, W. R. (1994) Molecular mechanics studies of model iron(III) transferrin complexes in vacuo and in aqueous solution. *Inorg. Chem. 33*, 884−890.
(49) Jorgensen, W. L., Chandrasekhar, J., Madura, J. D., Impey, R. W., and Klein, M. L. (1983) Comparison of simple potential functions for simulating liquid water. *J. Chem. Phys. 79*, 926−935.
(50) Bussi, G., Donadio, D., and Parrinello, M. (2007) Canonical sampling through velocity rescaling. *J. Chem. Phys. 126*, 014101.
(51) Darden, T., York, D., and Pedersen, L. (1993) Particle mesh ewald: An n.log(n) method for Ewald sums in large systems. *J. Chem. Phys. 98*, 10089−10092.
(52) Essmann, U., Perera, L., Berkowitz, M. L., Darden, T., Lee, H., and Pedersen, L. G. (1995) A smooth particle mesh Ewald potential. *J. Chem. Phys. 103*, 8577−8592.
(53) Hess, B., Bekker, H., Berendsen, H. J. C., and Fraaije, J. G. E. M. (1997) Lincs: A linear constraint solver for molecular simulations. *J. Comput. Chem. 18*, 1463−1472.
(54) Sakajiri, T., Yamamura, T., Kikuchi, T., Ichimura, K., Sawada, T., and Yajima, H. (2010) Absence of binding between the human transferrin receptor and the transferrin complex of biological toxic trace element, aluminum, because of an incomplete open/closed form of the complex. *Biol. Trace Elem. Res. 136*, 279−286.
(55) Mujika, J. I., Mercero, J. M., and Lopez, X. (2003) A theoretical evaluation of the pK_a for twisted amides using density functional theory and dielectric continuum methods. *J. Phys. Chem. A 107*, 6099−6107.
(56) Sun, X., Sun, H., Ge, R., Richter, M., Woodworth, R. C., Mason, A. B., and He, Q.-Y. (2004) The low pK_a value of iron-binding ligand Tyr188 and its implication in iron release and anion binding of human transferrin. *FEBS Lett. 573*, 181−185.
(57) Kurokawa, H., Mikami, B., and Hiroses, M. (1994) Crucial role of intralobe peptide-peptide interactions in the uptake and release of iron by ovotransferrin. *J. Biol. Chem. 269*, 6671−6676.
(58) James, N. G., Berger, C. L., Byrne, S. L., Smith, V. C., MacGillivray, R. T. A., and Mason, A. B. (2007) Intrinsic fluorescence reports a global conformational change in the N-lobe of human serum transferrin following iron release. *Biochemistry 46*, 10603−10611.

(59) Adams, T. E., Mason, A. B., He, Q.-Y., Halbrooks, P. J., Briggs, S. K., Smith, V. C., MacGillivray, R. T. A., and Everse, S. J. (2003) The position of arginine 124 controls the rate of iron release from the N-lobe of human serum transferrin. A structural study. *J. Biol. Chem. 278*, 6027−6033.
(60) *The PyMOL molecular graphics system*, version 1.3r1 (2010) Schrödinger, LLC, New York.